# *ALICE*: The ultraviolet imaging spectrograph aboard the *New Horizons* Pluto mission spacecraft

S. Alan Stern[a], John Scherrer[b], David C. Slater[b], G. R. Gladstone[b], Greg Dirks[b], John Stone[b], Michael Davis[b], Maarten Versteeg[b], and O. H. W. Siegmund[c]

[a]Southwest Research Institute, 1050 Walnut St., Suite 400, Boulder, CO 80302
[b]Southwest Research Institute, 6220 Culebra Rd., San Antonio, TX 78238
[c]Sensor Sciences, 3333 Vincent Road, Pleasant Hill, CA 94523

## ABSTRACT

The *ALICE* instrument is a lightweight (4.4 kg), low-power (4.4 W) imaging spectrograph that is planned to fly aboard the *New Horizons* mission to Pluto/Charon and the Kuiper Belt. Its primary job is to detect a variety of important atomic and molecular species in Pluto's atmosphere, and to determine their relative abundances as a function of altitude so that a complete picture of Pluto's atmospheric composition and structure can be determined for the first time. *ALICE* would also be used to search for an atmosphere around Pluto's moon, Charon, as well as the Kuiper Belt Objects (KBOs) that *New Horizons* hopes to fly by after Pluto-Charon. The *New Horizons ALICE* design, based on the *Rosetta ALICE* instrument design now en route to Comet 67P/ Churyumov-Gerasimenko aboard the European Space Agency's *Rosetta* spacecraft, incorporates an off-axis telescope feeding a Rowland-circle spectrograph with a 520-1870 Å spectral passband, a spectral point spread function of 3-6 Å FWHM, and an instantaneous spatial field-of-view of 6 degrees. Two separate input apertures that feed the telescope allow for both airglow and solar occultation observations during the mission. The focal plane camera is an imaging microchannel plate (MCP) double delay-line detector with dual solar-blind opaque photocathodes (KBr and CsI) and a focal surface that matches the 15-cm diameter Rowland-circle. Data taking modes include both histogram and pixel list exposures. We describe the scientific objectives of *ALICE* as well as the design, build, and environmental testing results of the flight model.

Keywords: UV spectroscopy, New Horizons, Pluto, Charon, Kuiper Belt Objects

## 1. INTRODUCTION

*New Horizons* (NH) is a scientific reconnaissance mission to the Pluto-Charon binary and possibly one or more Kuiper-Belt Objects (KBOs). It would launch from Kennedy Space Center (KSC) in January 2006,* with a backup launch window in January 2007. NH features an interlocking suite of sophisticated remote sensing and in situ instruments for science investigations during flybys of both Pluto-Charon and the KBO(s). The baseline January 2006 launch calls for a Jupiter gravity-assist trajectory that would flyby Jupiter in 2007, providing the opportunity for science observations of the Jupiter system. If launched during the optimum portion of the 2006 launch window, NH would reach Pluto-Charon in mid-2015 and perform science observations for ~150 days surrounding closest approach. Later launches in 2006 and 2007 could result in Pluto-Charon encounters during 2016 to 2021.

The remote sensing instruments aboard NH include two visible light imaging cameras (called *RALPH* and LORRI), an IR imaging spectrograph (called LEISA), a thermal radiometer (called REX), and an ultraviolet (UV) imaging spectrograph called *ALICE*. *ALICE* is a low-cost instrument designed to perform spectroscopic investigations of planetary atmospheres and surfaces at extreme (EUV) and far-ultraviolet (FUV) wavelengths between 520 and 1870 Å. *ALICE* is a direct derivative of the Pluto mission HIPPS UV spectrograph (HIPPS/UVSC), developed at Southwest Research Institute (SwRI) and breadboarded with funds from NASA, JPL, and SwRI[1]. The HIPPS/UVSC instrument was subsequently optimized for the European Space Agency (ESA) *Rosetta* mission by increasing its sensitivity, instantaneous field-of-view (FOV), and wavelength coverage, and by adding a lightweight microprocessor. This

* The NH mission launch date is contingent upon NASA completing the federally mandated NEPA Environmental Impact Statement and its associated Record of Decision, as well as the reviews required by Presidential Directive National Security Council PD/NSC-25, for launch approval.

Astrobiology and Planetary Missions, edited by Richard B. Hoover, Gilbert V. Levin, Alexei Y. Rozanov, G. Randall Gladstone, Proc. of SPIE Vol. 5906, 590618, (2005) · 0277-786X/05/$15 · doi: 10.1117/12.613128

instrument, called *Rosetta-ALICE* (*R-ALICE*)[2], was successfully launched on the *Rosetta* spacecraft in March 2004, and is operating successfully on a 10-year mission to rendezvous with and orbit about comet 67P/Churyumov-Gerasimenko. An improved derivative of *R-ALICE* was designed, built and tested for the *New Horizons'* remote sensing suite; improvements include an entrance aperture for airglow channel (AGC) observations and a solar occultation channel (SOC) for direct solar observations at 30 AU. The SOC provides for solar occultation observations through Pluto's atmosphere during the NH flyby, and allows the most sensitive test available for an atmosphere surrounding Charon and the targeted Kuiper Belt Object(s). The scientific objectives of the NH *ALICE* (also called *P-ALICE*) as well as a description of the instrument are presented in this paper. Radiometric test performance results of the *P-ALICE* flight model are given in Slater *et al.*[3].

## 2. SCIENTIFIC OBJECTIVES

One of the three primary (i.e., Group 1) mission objectives for NH is to "Characterize the neutral atmosphere of Pluto and its escape rate". *P-ALICE* is designed to address this measurement objective. In particular, *P-ALICE* addresses various important questions about Pluto's atmosphere, including:

- What are the mixing ratios of $N_2$, CO, $CH_4$, H, and noble gases?
- What is the vertical density and temperature structure of the upper atmosphere?
- Is the steepening of the stellar occultation light curve observed in 1988[4] caused by low-altitude hazes, or thermal gradients, or both?
- What drives hydrocarbon and nitrile photochemistry?
- What is the atmospheric escape rate?
- Is bulk hydrodynamic escape really taking place?

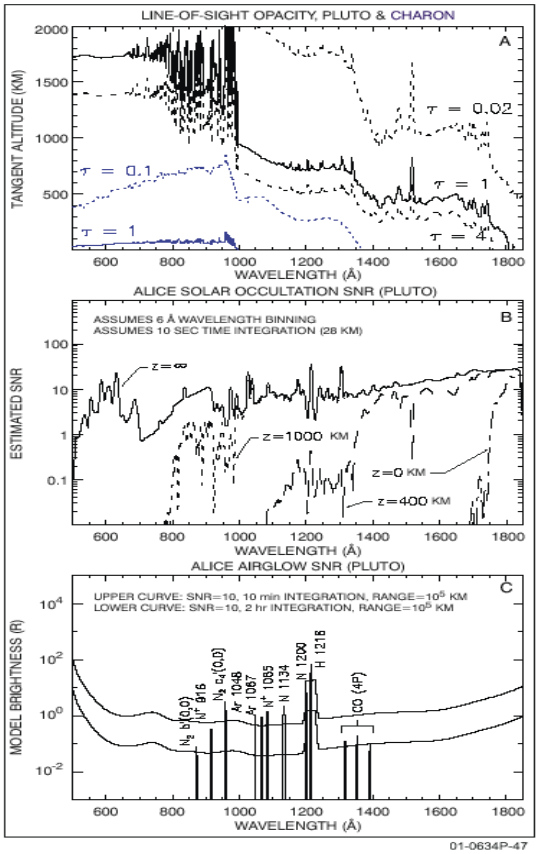


**Figure 1.** a) Limb-viewing, line-of-sight opacity for model Pluto (black) and Charon (blue) atmospheres are shown as a function of wavelength and tangent altitude, for several values of τ; b) Estimated SNR based on the line-of-sight transmitted solar flux through Pluto's atmosphere, for several tangent altitudes, as a function of wavelength (integration times of 10s are assumed); c) Model dayglow brightnesses for several emissions resulting from photoelectron impact excitation, dissociative excitation, and resonant scattering of sunlight. The upper and lower curves show the expected *P-ALICE* SNR~10 for 10-minute and 2-hour integrations at a range of $10^5$ km.

*P-ALICE* employs airglow and solar occultation spectra to address these and other relevant questions about Pluto's atmosphere. Figure 1 shows results of modeling for solar occultation and airglow observations by *P-ALICE,* based on published model results for Pluto's atmosphere[5]. The continuum and band absorption structure of $N_2$ at wavelengths <100 nm dominates the EUV opacity and allows sampling of the uppermost atmosphere. From 100-150 nm, $CH_4$ dominates the opacity, providing a window on the middle atmosphere from roughly 300 to 1200 km. At wavelengths >150 nm, higher hydrocarbons with strong FUV absorption bands, such as $C_2H_2$ and $C_4H_2$ are expected to be optically important, and, along with hazes, are expected to provide information about the lowest few 100 km of the atmosphere. Pluto's atmospheric temperature profile is believed to rise steeply from the surface with the first 10 km of altitude (at up to 15 K/km), due to absorption of near-IR solar radiation by methane bands, quickly reaching the value of 102±9 K determined from the 1988 stellar occultation data. Heating by Lyman-α photodissociation (from both the Sun and the interstellar medium (ISM) in roughly similar amounts) may increase the temperature to about 120 K at altitudes near 600 km. At even higher altitudes (near 1000 to 1500 km), absorption of solar EUV radiation by $N_2$ provides additional heating, but

the atmospheric temperature likely decreases above 600 km due to cooling associated with hydrodynamic escape[5]. Pluto is unique among the planets in that its atmosphere is not just boiling away (e.g., from classical Jean's escape), but is actually thought to be blowing away by hydrodynamic escape, much as gases escape from comets. Most studies have put the total escape rate (referred to the surface) at a few times $10^{10}$ $cm^{-2}$ $s^{-1}$ (i.e., a few km of $N_2$ ice over the age of the solar system).

Hydrocarbon photochemistry, initiated by the photodissociation of $CH_4$ by Lyman-α, is expected to produce substantial quantities of condensable species, including acetylene ($C_2H_2$), diacetylene ($C_4H_2$), hydrogen cyanide (HCN), cyanoacetylene ($HC_3N$), ethane ($C_2H_6$), and ethylene ($C_2H_4$). Whether these species measurably precipitate onto the surface depends on the strength of hydrodynamic escape and other factors. Although the heavier of these species are expected to preferentially precipitate, none of these species have been observed as surface ices to date. The lighter photochemical products are likely to participate in the planet's escaping wind. One way to investigate the strength of the wind is to determine the mixing ratio profiles of the minor atmospheric species in the 500—1500 km altitude region, since under weak wind conditions the mixing ratios of the minor species would vary more in accordance with diffusive equilibrium, while for a strong wind the mixing ratios would be relatively constant with altitude.

The abundance of argon in Pluto's atmosphere is a compelling open question. Although it is unlikely to be the dominant constituent, an Ar mixing ratio of several percent is not an unreasonable expectation. The model Pluto atmosphere used in Fig. 1 assumes 5% Ar abundance, which *P-ALICE* can rather easily detect. As alluded to above, an aerosol haze, perhaps photochemically produced, is considered likely in the lower atmosphere, and may mitigate the need for a large near-surface temperature gradient required to fit the occultation data as mentioned above. Based on comparison with Triton, haze optical depths on the order of $10^{-3}$ might be expected.

The remainder of the paper describes the instrument design and functionality.

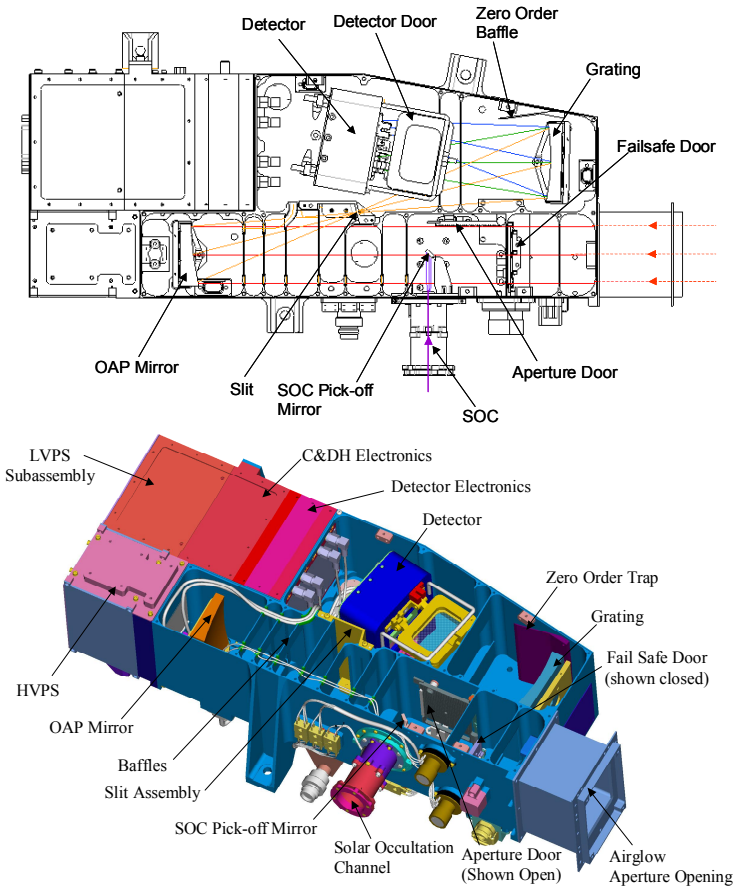


**Figure 2.** (Top) An opto-mechanical of *P-ALICE* showing light rays traced through the AGC and SOC apertures. (Bottom) 3-D opto-mechanical view of *P-ALICE*.

## 3. INSTRUMENT DESCRIPTION

### 3.1. Overview

The *P-ALICE* UV spectrograph is a relatively simple instrument comprised of a telescope and a Rowland-circle spectrograph. An opto-mechanical layout of the instrument is shown in Figure 2. *P-ALICE* has two separate entrance apertures that feed light to the telescope section of the instrument: the airglow channel (AGC) aperture and the solar occultation channel (SOC) aperture. The former is a 40 x 40 $mm^2$ entrance aperture at the front end of the instrument; the latter is a small 1-mm diameter opening located perpendicular to the side of the telescope section of the instrument (see Fig. 2). Light entering either aperture is collected and focused by an f/3 off-axis paraboloidal (OAP) primary mirror at the back end of the telescope section onto the instrument's entrance slit*. After passing through the entrance slit, the light falls onto a toroidal holographic diffraction grating, which disperses the light onto a double-delay line (DDL) microchannel plate (MCP) detector[6]. The 2-D (1024 x 32)-pixel format MCP detector uses dual, side-by-side, solar-blind photocathodes—potassium bromide (KBr) and cesium iodide (CsI)—and has a cylindrically-curved MCP-stack that matches the Rowland-circle. *P-ALICE* is controlled by an Intel 8052 compatible microcontroller, and utilizes lightweight, compact, surface mount electronics to support the science detector, as well as the power supply, command and data handling, instrument support, and some other spacecraft interface electronics. Figure 3 shows a photograph of the exterior of the *P-ALICE* flight model. The resulting design is highly systems-engineered to minimize mass and complexity, and enjoys strong parts-level heritage from previous UV spectrographs.

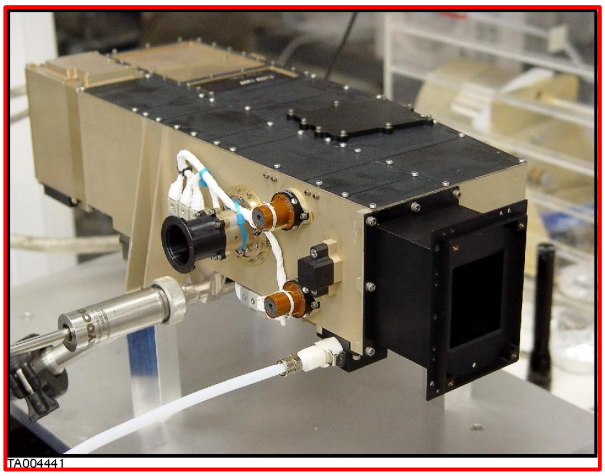


**Figure 3.** Photograph of the *P-ALICE* flight model.

### 3.2. Opto-mechanical Design

The OAP mirror and diffraction grating are constructed from monolithic pieces of aluminum, coated with electroless nickel and polished using low-scatter polishing techniques. The aluminum optics, in conjunction with the aluminum housing, form an athermal optical design. Both optics are overcoated with sputtered SiC for optimum reflectivity within the *P-ALICE* EUV/FUV spectral passband[7]. Besides using low scatter optics, additional control of internal stray light is achieved using internal baffle vanes within both the telescope and spectrograph sections of the housing, a holographic diffraction grating that has low scatter and near-zero line ghost problems, and an internal housing with alodyned aluminum surfaces[8,9]. In addition, the zero order baffle light trap is treated with a nickel-phosphorus (Ni-P) black coating with very low surface reflectance at EUV/FUV wavelengths[10].

A number of preventative measures reduce the risk of instrument contamination. Heaters are mounted to the back surfaces of the OAP mirror and grating to prevent condensation of contaminants during flight. To protect the sensitive photocathodes and MCP surfaces from exposure to moisture and other harmful contaminants during ground operations, instrument integration, and the early stages of the mission, the detector tube body assembly is enclosed in a vacuum chamber with a front hermetic door that includes a magnesium fluoride ($MgF_2$) UV-transparent window that is permanently opened during the commissioning phase of the flight. The front aperture door can be commanded closed for additional protection of the optics and detector from direct solar exposure during possible spacecraft maneuvers.

The spectrograph entrance slit assembly design is shown in Figure 4. The slit is composed of two contiguous sections: a narrow AGC slit with a field-of-view of 0.1º x 4.0º; and a SOC slit with a square field-of-view of 2.0º x 2.0º. The AGC slit is used for airglow and surface albedo studies; it encompasses the center boresight and provides an extended source spectral resolution of ~9 Å(3). The large SOC slit opening, on the other hand, is designed to ensure that the Sun is captured within the instrument's field-of-view during the solar occultation observations of Pluto and Charon that must occur nearly simultaneously with the radio science occultation observations performed with the NH REX instrument and the spacecraft's high gain antenna (HGA). During solar occultation observations, the HGA would be

* A small flat relay mirror redirects light entering the SOC to the OAP primary mirror.

pointed back at the Earth, with *P-ALICE* pointed back at the Sun. *P-ALICE* is aligned on the spacecraft with a 2º tilt along the spectrograph's spatial axis so that the Sun is centered within the SOC square FOV when the HGA is pointed at the Sun (to improve the quality of the radio occultation data, the flyby is planned to occur when Pluto is near opposition as seen from Earth, i.e., around mid-July). Any misalignment up to ±0.9º between the SOC FOV and the HGA boresight can be accommodated with the large SOC FOV. The spectral PSF of the SOC is ~5 Å across the passband[3]. The SOC and AGC may also be used for stellar occultations of flyby targets.

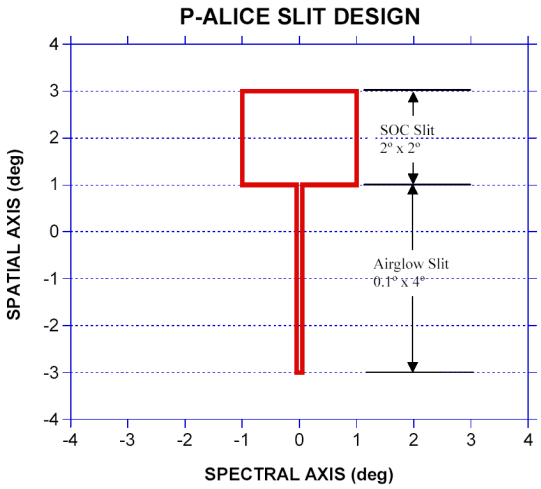


**Figure 4.** The *P-ALICE* entrance slit design. The narrow 0.1º x 4º slit is designated the "airglow" slit; the larger 2º x 2º opening above the airglow slit is the SOC slit. The airglow optical boresight is centered at (0º, 0º).

*P-ALICE* has five "one-time use" actuators: 1) an aperture door launch latch (secures the aperture door during launch); 2) a failsafe door; 3) a SOC door; 4) a detector door; and 5) a detector housing vent valve. The first three of these utilize TiNi shaped memory alloy (SMA) pin-puller actuators. The detector door utilizes a wax pellet actuator (WPA), and the vent valve is a simple latching solenoid valve. The aperture door is the sole multiple use actuator, and can be opened and closed via telecommand to the command-and-data handling (C&DH) electronics. A limited angle torque (LAT) motor with a direct tie to the aperture door hinge pin provides the torque required to open and close the door. The aperture door remains closed until it is determined that the spacecraft has had sufficient time to fully outgas. The aperture door is then opened to allow residual outgassing of the interior of the instrument and for heater decontamination sessions of the optics. Following these activities, the detector door is opened with the WPA followed by a slow, controlled, high voltage ramp up of the detector MCP stack to begin detector check out. Detector dark/background measurements with the aperture door closed and Lyman-α skyglow measurements with the aperture door open take place as part of detector functionality tests. These measurements are followed by raster and step-stare scans of UV stars are performed to check the instrument sensitivity for in-flight calibration purposes. Later in the flight, the SOC door would be opened and sensitivity checks of the SOC channel performed, again using hot UV stars.

A failsafe aperture door opening would only be used if the aperture door ever became stuck in the closed state. With the failsafe door open, the AGC sensitivity is ~10% that of the fully opened AGC with the aperture door in the open state. Likewise, the detector vent valve, located along the detector pump-out tube, would only be opened if the detector door does not open. Firing the vent valve allows any residual gas within the detector housing to vent to space to allow safe high voltage operation with the detector door closed.

### 3.3. Detector and Detector Electronics

The 2-D imaging photon-counting detector located in the spectrograph section of the instrument utilizes an MCP Z-stack that feeds the DDL readout array[6]. The input surface of the Z-stack is coated with opaque photocathodes of KBr (520-1180 Å) and CsI (1250-1870 Å)[11]. The detector tube body is a custom design made of a lightweight brazed alumina-Kovar structure that is welded to a housing that supports the DDL anode array.

To capture the entire 520-1870 Å passband and 6° spatial FOV, the size of the detector's active area is 35 mm (in the dispersion direction) x 20 mm (in the spatial dimension), with a pixel format of (1024 x 32)-pixels. The 6° slit-height is imaged onto the central 22 of the detector's 32 spatial channels; the remaining spatial channels are used for dark count monitoring. Our pixel format allows Nyquist sampling with a spectral resolution of 3.6 Å, and a spatial resolution of ~0.6°.

The MCP Z-stack is composed of three 80:1 length-to-diameter (L/D) MCPs that are cylindrically curved with a radius-of-curvature of 75 mm to match the Rowland-circle for optimum focus. The total Z-Stack resistance is ~300 MΩ. The MCPs are rectangular in format (46 x 30 $mm^2$), with 12-μm diameter pores. Above the MCP Z-Stack is a repeller grid that is biased ~900 V more negative than the top of the MCP Z-Stack. This repeller grid reflects electrons liberated in the interstitial regions of the MCP back down to the MCP input surface to enhance the detector quantum efficiency. The MCP Z-stack requires a high negative voltage bias of ~ –3 kV; an additional –600 V is required between the MCP

Z-stack output and the anode array (the anode array is referenced to ground). The dark count rate of the flight MCP stack is quite low and stable—less than 3 c/s over the entire MCP active area[3].

To prevent saturation of the detector electronics during the solar occultation observations, it is necessary to attenuate the solar Lyman-α emission brightness to an acceptable count rate level well below the maximum count rate capability of the electronics (i.e., below $3\times10^4$ c $s^{-1}$). An attenuation factor of at least an order of magnitude is required to achieve this lower count rate. This attenuation is easily achieved by physically masking the MCP active area where the H I Lyman-α emission comes to a focus during the photocathode deposition process. The bare MCP glass has a quantum efficiency about 10 times less than that of KBr at 1216 Å. This masking technique has been successfully demonstrated in the past with the DDL detector aboard the *Rosetta-ALICE* instrument[2], as well as other spaceflight UV instruments such as the SUMER instrument on SOHO[12].

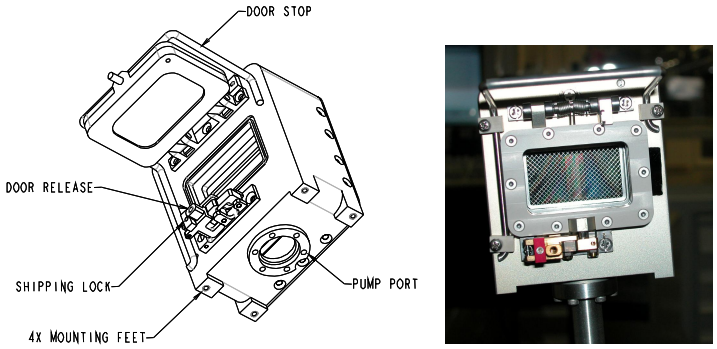


**Figure 5.** (Left) 3-D schematic of DDL detector vacuum housing with the detector door shown in the open position. (Right) Photograph of the flight DDL detector/vacuum housing. The repeller mesh and MCP Z-stack are visible through the $MgF_2$ window.

Surrounding the detector tube body is the vacuum chamber housing made of aluminum and stainless steel (see Figure 5). As mentioned above, this vacuum chamber is designed to protect the KBr and CsI photocathodes against damage from moisture exposure during ground handling and from outgassing constituents during the early stages of flight. It also allows the detector to remain under vacuum during ground operations, testing & handling, and transportation. The MCP/anode tube body assembly mounts to the rear stainless steel vacuum flange. This flange mates to the aluminum vacuum housing with a vacuum tight O-ring seal, and contains two high-voltage (HV) feedthrough connectors that are welded to the flange (HV input and return), as well as four welded microdot feedthrough connectors for the four analog signal outputs from the DDL anode.

Light enters the detector vacuum chamber through an openable door which contains a built-in $MgF_2$ window port to transmit UV light at wavelengths >1200 Å. This window allows testing of the detector with the door closed and provides redundancy during flight if the door mechanism fails to deploy. The housing also has a built-in pump-out port connected to a pump-out tube (POT) with a small valve used to isolate the detector after pumpdown. The detector is pumped out through this tube with a GSE vacuum pump station, and vacuum is maintained with a red-tagged 2 L $s^{-1}$ GSE detachable vacuum-ion pump.

The detector door should be opened only once during flight, using a torsion spring released by the WPA. The detector door design is an improved version of that flying aboard the *R-ALICE* instrument[2]. During ground operations the door can be opened numerous times and manually reset; during flight, once open, the door need not and cannot be re-closed.

The detector electronics include preamplifier circuitry, time/charge digital converter circuitry (TDC), and pulse-pair analyzer circuitry (PPA). All of these electronics are packaged into three 63.5 x 76.2 $mm^2$ boards using surface-mount components. These three boards are mounted inside a separate enclosed aluminum housing that mounts to the rear of the spectrograph section (just behind the detector vacuum chamber). The detector electronics require ± 5 VDC, and draw ~1.1 W.

The detector electronics amplify and convert the detected output pulses from the MCP Z-stack to pixel address locations. Only those analog pulses output from the MCP that have amplitudes above a set threshold level are processed and converted to pixel address locations. For each detected and processed event, a 10-bit *x* (spectral) address and a 5-bit *y* (spatial) address are generated by the detector electronics and sent to the *P-ALICE* C&DH electronics for data storage and manipulation. In addition to the pixel address words, the detector electronics also digitizes the analog amplitude of each detected event output by the preamplifiers and sends this data to the C&DH electronics. Histogramming of this "pulse-height" data creates a pulse-height distribution used to monitor the health and status of the detector during operation.

A built-in "stim-pulser" is also included in the electronics that simulates photon events at two pixel locations on the array (located in the upper right and lower left corners of the active array). This pulser can be turned on and off by command and allows testing of the entire *P-ALICE* detector and C&DH electronic signal path without having to power on the detector high-voltage power supplies or put light on the detector.

Finally, an analog count rate signal is output from the detector electronics to the C&DH to allow monitoring and recording of the detector total array count rate. This count rate data is updated once per second and is included in the instrument housekeeping (HK) data.

### 3.4. Instrument Electrical Design

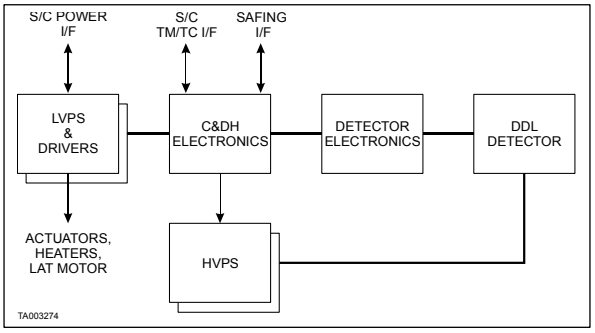


**Figure 6.** Simplified electronics block diagram of *P-ALICE*.

The *P-ALICE* instrument support electronics include the low-voltage power supply (LVPS) and actuator electronics, the C&DH electronics, the optics decontamination heater system, and the redundant detector high-voltage power supplies (HVPSs). A simplified block diagram of how all these electronic subsystems are interfaced to each other is shown in Figure 6. All of these sub-systems are controlled by a radiation-hardened version of the Intel 8052 microprocessor with 32 kB of fuse programmable PROM, 128 kB of EEPROM, 32 kB of SRAM, and 128 kB of acquisition memory. The C&DH electronics are contained on four circuit boards located just behind the detector electronics (see Figure 2). A detailed block diagram of these electronics is shown in Figure 7.

We now present a brief description of the LVPS, C&DH, decontamination heater system, and the HVPS electronics.

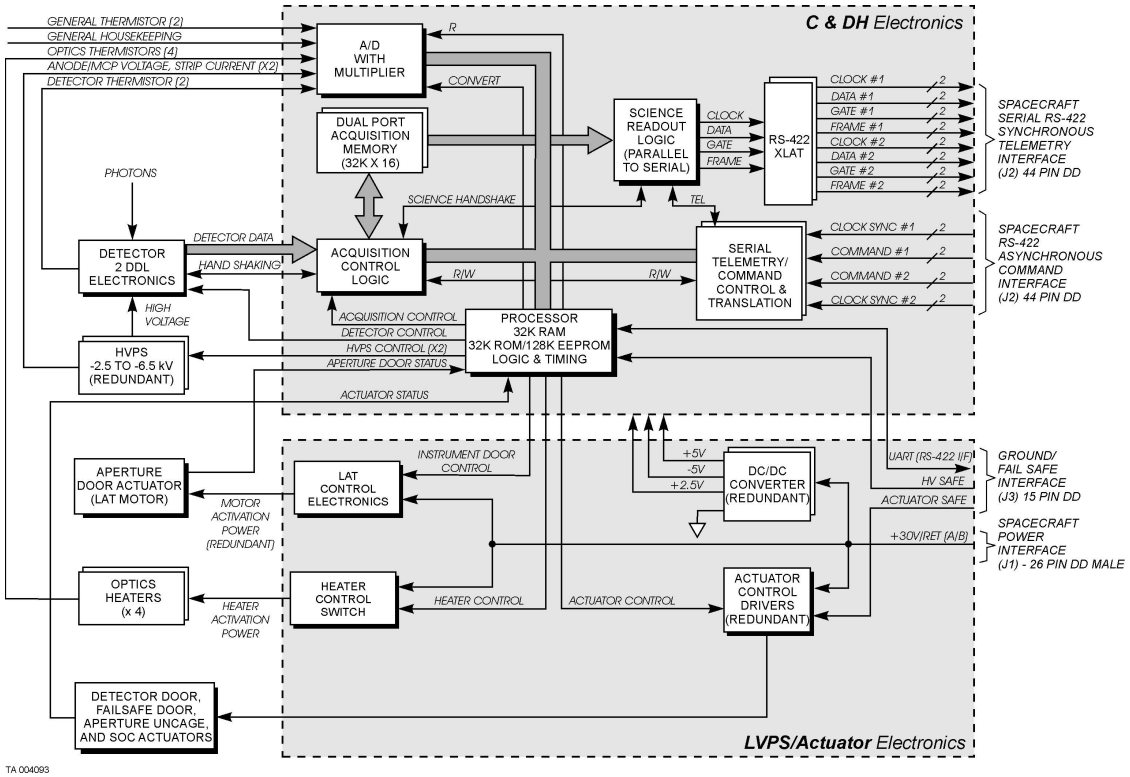


**Figure 7.** Detailed block diagram of *P-ALICE*.

*Low-Voltage Power Supply Electronics.* The LVPS electronics and associated drivers are dual redundant, and are each composed of DC/DC converters designed to convert the +30V supplied spacecraft power to ± 5 VDC (power ~4 W) and +2.5 VDC (power ~0.4 W) required by the detector electronics, the C&DH, and the detector HVPSs. Five boards make up the LVPS: two LVPS boards (primary and redundant); an EMI filter board; a heater/actuator board; and a motherboard. The LVPS electronics interfaces to the spacecraft via three links: two links to the +30V spacecraft power bus for a) instrument power and b) actuator/heater power; the third link is a safing connector interface that prevents inadvertent HVPS and/or actuator (i.e., launch latch, detector door, fail-safe door, SOC door, and/or detector vent valve) operations. The switching circuit for the decontamination heaters and the LAT motor controller that operates the front aperture door is also located in the LVPS electronics.

*High Voltage Power Supplies.* Dual-redundant HVPSs are located in a separate enclosed bay behind the OAP primary mirror (see Figure 2). The HV output of these two supplies are diode-or'd together to the single HV terminal on the MCP/anode assembly. Each supply can output a maximum of –6 KV to the top of the MCP/repeller grid assembly—well above the nominal operational HV level of –4.5 kV. The voltage between the MCP output and the anode array is fixed at –600 V using zener diodes between the output and ground. The voltage to the MCP Z-stack is fully programmable by command between 0 and –6 kV. The mass of the two supplies is ~460 grams. They require ±5 VDC and consume ~0.3 W.

*Command–and–Data–Handling Electronics.* The C&DH electronics, which are controlled by the 8052 microprocessor, provide the command interface as well as the science and telemetry interfaces with the spacecraft. Specifically, they handle the following instrument functions: (i) interpretation and execution of commands to the instrument, (ii) collection of raw event data from the detector to the dual port acquisition memory (see Fig. 7) in either the pixel list or histogram data collection modes (described in the following section), (iii) telemetry formatting of science and housekeeping data, (iv) control of the dual-redundant detector HVPSs, (v) operation of all actuator and heater functions, (vi) control of the front aperture door LAT motor, (vii) control of the housekeeping ADCs used to convert analog housekeeping data to digital data for inclusion into the TM data stream, and (viii) monitoring of detector health and status via the detector analog count rate, and the HVPSs' high voltage and MCP strip current values. For *P-ALICE* flight operations, the Intel 8052 microprocessor operates with a clock frequency of 4.0 MHz.

The *P-ALICE* low-speed HK telemetry and telecommand interface is via an RS-422 asynchronous interface to the spacecraft. A second FPGA within the C&DH electronics controls this low-speed data flow.

*Decontamination Heater System.* A single decontamination heater (~1 W resistive) is bonded to the backside surface of both the OAP mirror and the grating substrates. Along with each heater, two redundant thermistors are also mounted to the back of each substrate to monitor and provide control feedback to the heaters. The C&DH electronics can separately control each heater. The decontamination heaters would be activated periodically during flight, with planned activations early in the mission during the commissioning phase, and during annual instrument checkout opportunities during the long cruise to Pluto/Charon and the KBO(s).

### 3.5. Data Collection Modes

Science data from the detector is collected in the dual port acquisition memory that consists of two separate 32k x 16-bit memory channels. *P-ALICE* has two detector data collection modes described in detail below: i) *pixel list mode*; and ii) *histogram mode*. The *P-ALICE* flight software controls both of these modes.

In *pixel list mode* each memory channel can hold up to 32k detector and/or time-hack events; where each detector event consists of a 16-bit word—an *x*-position word 10 bits in length, a *y*-position word 5 bits in length, and a single status bit that distinguishes between a time hack word and a detector event word; a time hack word includes a single status bit plus 15-bits that encodes the instrument on-time. When 32k detector address and time-hack events have accumulated in one of the two acquisition memories, that acquisition memory stops accumulating event data and begins to read the data out to a parallel-to-serial converter and a low-voltage differential signaling (LVDS) interface to the spacecraft on-board memory. At the same time that this LVDS readout is taking place, the other side of the dual acquisition memory continues to collect detector and time-hack data until it fills up, whereupon it reads out to the LVDS interface to the spacecraft memory, while the first acquisition memory takes over collecting detector and time-hack data. This back-and-forth data collection flow between both acquisition memories is called "ping-pong" acquisition—it allows contiguous readout of detector event data as long as the data event rate does not exceed the rate at which the data can be read out of memory to the LVDS interface. The "ping-pong" acquisition process is controlled using logic encoded in one of two FPGAs within the C&DH electronics.

In *histogram mode*, each memory location represents a pixel location in the detector 2-D 1024 x 32 array. When a detector event address is sent from the detector to the C&DH, the acquisition control logic updates the proper pixel address location in memory with a single additional count. Since there are 32k pixels in the detector array, each memory address can hold up to $(2^{16} - 1)$ events before the counter saturates at this maximum value. When a single histogram exposure is complete, the memory is read out to the LVDS interface to the spacecraft. A second exposure can then begin using the other acquisition memory bank while the first bank is reading out to the spacecraft. Besides the collection and binning of detector events, histogram mode allows the collection of MCP pulse-height distribution (PHD) data from the detector electronics. This PHD data is collected and binned into a 64-bin histogram that is stored within the first two rows of the detector histogram, in a location where no physical pixel within the detector active area exists (therefore, the PHD data does not interfere with the collected detector data). The same C&DH FPGA that controls the pixel-list "ping-pong" acquisitions also controls the histogram data collection mode.

*P-ALICE* also includes a mechanism to filter out events from selected areas of the detector. This may be used to suppress 'hot pixels' that could develop in the detector, especially in the pixel list mode, which might otherwise consume a large fraction of the available acquisition memory. This filtering is performed before events are processed in either histogram or pixel list mode. The system defines up to 8 rectangular regions of 32 by 4 pixels that suppress any events from the selected regions from being processed. Configuration parameters allow for the placement of these filters areas at any desired positions within the detector area.

### 3.6. Performance Summary

The flight *P-ALICE* model was subjected to an environmental test program following the completion of the instrument fabrication and integration activities, which included instrument vibration, electromagnetic interference (EMI) and thermal-vacuum testing. Following these test activities, *P-ALICE* underwent a thorough radiometric characterization and absolute calibration at the SwRI UV Vacuum Calibration facility. Detailed results of this testing are described in Slater *et al.*[3]. Table I provides the measured performance values and compares these with the requirement values. All the radiometric requirements and goals were met and verified.

***Table I*—P-ALICE *Radiometric Test Performance Summary***

| **Radiometric Test** | **Test Requirement/Goal** | **Measured Values** |
|---|---|---|
| Dark count rate | ≤ 1 $cm^{-2}$ $s^{-1}$ (total array) | 0.3 $cm^{-2}$ $s^{-1}$ (total array) |
| Wavelength calibration | < 1 Å calibration precision | ±0.62 Å (1σ using a linear fit) |
| PSF vs. λ (airglow & SOC) | < 6 Å (SOC)<br>< 18 Å (airglow)<br>< 2 spatial pixels (spatial) | 3.0-3.5 Å (SOC)<br>3.0-4.5 Å (airglow)<br>0.4-1.5 spatial pixels (spatial) |
| Wavelength passband | 520-1870 Å (minimum coverage) | 465-1881 Å |
| Filled slit spectral resolution | < 18 Å FWHM (airglow) | 9.0 ± 1.4 Å (FWHM) |
| Spectral plate scale | 1.7 ± 0.2 Å/pixel | 1.832 ± 0.003 Å/pixel |
| Spatial plate scale | < 0.30 per spatial pixel | 0.27° ± 0.01° |
| Off-axis light scatter test (airglow) | PST* < $10^{-6}$ at $\theta_{off}$ > 7º | PST < 4.6 x $10^{-8}$ at $\theta_{off}$ > 7º (spectral axis)<br>PST < 8.3 x $10^{-7}$ at $\theta_{off}$ > 7º (spatial axis) |
| H Lyman α attenuation/scatter | < 10% (total integrated scatter; goal) | TIS = 2.4% (outside PC gap) |
| H Lyman α gap λ boundaries | Δλ ~ 70-75 Å centered at 1216 Å | Gap: 1178.6 Å to 1251.9 Å (Δλ = 73.3 Å)† |
| Absolute effective area (airglow values) | 650-800 Å : >0.03 $cm^2$<br>1000-1100 Å : >0.07 $cm^2$<br>1181-1251 Å: 0.003-0.03 $cm^2$<br>1300-1400 Å: >0.01 $cm^2$<br>1600-1750 Å: >0.03 $cm^2$ | 650-800 Å : 0.07-0.17 $cm^2$<br>1000-1100 Å : 0.20-0.30 $cm^2$<br>1181-1251 Å: 0.02 $cm^2$<br>1300-1400 Å: 0.15-0.18 $cm^2$<br>1600-1750 Å: 0.03-0.05 $cm^2$ |
| SOC relative effective area | < 1/2500 of AGC effective area** | 1/7300 to 1/3000 of AGC effective area |

*PST = Point Source Transmittance = $E_{det}/E_{in}$, where $E_{det}$ is the irradiance at the detector; $E_{in}$ is the input irradiance.

** Assumes a nominal AGC effective area.

† With point source centered in AGC slit; gap pixel boundaries: cols 525.5 to 565.4 at room temperature,+22º C)

## 4. CONCLUDING REMARKS

*New Horizons* is being planned for a launch opportunity in January 2006, with a flyby of Jupiter in February 2007, and a Pluto-Charon encounter in July 2015. In-flight calibration is planned for *P-ALICE* during the early phases of the mission to characterize its in-flight performance. Observations of hot UV stars (as well as the Sun and Jupiter) would be observed with *P-ALICE* to provide in-flight calibration. Science observations would be made during the Jupiter flyby, including synoptic observations of the Io Plasma Torus and the Jovian aurora and airglow. At Pluto, the key observations would be the solar occultation of Pluto's atmosphere and Charon, and airglow observations of important species to determine the structure and composition of the atmosphere from the near surface to high altitude.

## ACKNOWLEDGEMENTS

We thank the *P-ALICE* engineering and support team at SwRI, John Vallerga and Rick Raffanti at Sensor Sciences, and our French collaborators for providing optics. This work was supported by NASA contract #NASW02008.

## REFERENCES

1. Stern, Alan, David C. Slater, William Gibson, Harold J. Reitsema, Alan Delamere, Donald E. Jennings, Dennis C. Reuter, John T. Clarke, Carolyn C. Porco, Eugene M. Shoemaker, and John R. Spencer, "The Highly Integrated Pluto Payload System (HIPPS): A Sciencecraft Instrument for the Pluto Mission," in *EUV, X-Ray, and Gamma-Ray Instrumentation for Astronomy VI*, Proceedings of SPIE Vol. **2518**, O.H.W. Siegmund and John Vallerga, Editors, 39-58 (1995).
2. Slater, D. C., S. A. Stern, T. Booker, J. Scherrer, M. F. A'Hearn, J. L. Bertaux, P. D. Feldman, M. C. Festou, and O. H. W. Siegmund, "Radiometric and calibration performance results for the Rosetta UV imaging spectrometer *ALICE*," in *UV/EUV and Visible Space Instrumentation for Astronomy and Solar Physics*, Oswald H. W. Siegmund, Silvano Fineschi, Mark A. Gummin, Editors, Proceedings of SPIE Vol. **4498**, 239-247 (2001).
3. Slater, D. C., M. W. Davis, C. B. Olkin, S. A. Stern, and J. Scherrer, "Radiometric performance results of the *New Horizons' ALICE* UV imaging spectrograph," in *X-Ray, UV, Visible, and IR Instrumentation for Planetary Missions*, Oswald H. W. Siegmund and G. Randall Gladstone, Editors, Proceedings of SPIE Vol. **5906B**, (2005).
4. Elliot, J. L., E. W. Dunham, A. S. Bosh, S. M. Slivan, L. A. Young, and L. H. Wasserman, "Pluto's atmosphere," *Icarus*, **77**, 148 (1989).
5. Krasnopolsky, V. A., and D. P. Cruikshank, "Photochemistry of Pluto's atmosphere and ionosphere near perihelion," *J. Geophys. Res.*, **104**, (E9), 21,979-21,996, 1999.
6. Siegmund, O. H. W., J. Stock, R. Raffanti, D. Marsh, and M. Lampton, "Planar Delay Line Readouts for High Resolution Astronomical EUV/UV Spectroscopy," in *UV and X-Ray Spectroscopy of Astrophysical and Laboratory Plasmas*, Proceedings from the 10th International Colloquium, Berkeley, CA 3-5 February 1992, 383-386 (1992).
7. Osantowski, J.F., R.A.M. Keski-Kuha, H. Herzig, A.R. Toft, J.S. Gum, and C.M. Fleetwood, "Optical Coating Technology for the EUV," *Adv. Space Res*., **11**, (11), 185-201 (1991).
8. Jelinsky, Patrick, and Sharon Jelinsky, "Low reflectance EUV materials: a comparative study," *Appl. Opt.*, **26**, 4, 613-615, (1987).
9. Moldosanov, K. A., M. A. Samsonov, L. S. Kim, R. Henneck, O.H. W. Siegmund, John Warren, Scott Cully, and Dan Marsh, "Highly absorptive coating for the vacuum ultraviolet range," *Appl. Opt*., **37**, 1, 93-97 (1998).
10. Brown, Richard J. C., Paul J. Brewer, and Martin J. T. Milton, "The physical and chemical properties of electroless nickel-phosphorus black surfaces," *J. Mater. Chem*., **12**, 2749-2754 (2002).
11. Siegmund, O. H. W., "Microchannel Plate Imaging Detector Technologies for UV Instruments," in Conference Proceedings *From X-rays to X-band—Space Astrophysics Detectors and Detector Technologies*, Space Telescope Science Institute, (2000).
12. Siegmund O.H., Stock J.M., Marsh D.R., Gummin M.A., Raffanti R., Hull J., Gaines G.A., Welsh B.Y., Donakowski B., Jelinsky P.N., Sasseen T., Tom J.L., Higgins B., Magoncelli T., Hamilton J.W., Battel S.J., Poland A.I., Jhabvala M.D., Sizemore K., Shannon J., "Delay-line detectors for the UVCS and SUMER instruments on the SOHO Satellite," in *EUV, X-Ray, and Gamma-Ray Instrumentation for Astronomy V*, Oswald H. W. Siegmund, John V. Vallerga, Editors, Proceedings of SPIE Vol. **2280**, 89-100 (1994).
13. Danzmann, K., M. Günther, J. Fischer, M. Kock, and M. Kühne, "High current hollow cathode as a radiometric transfer standard source for the extreme vacuum ultraviolet," *Applied Optics*, **27**, 4947-4951 (1988).